JGR Solid Earth

RESEARCH ARTICLE
10.1029/2021JB022595

3-D Structure and Development of a Metamorphic Core Complex in the Northern South China Sea Rifted Margin

Qing Ye[1], Lianfu Mei[1], Dapeng Jiang[2], Xinming Xu[2], Efstratios Delogkos[3], Lili Zhang[2], and Giovanni Camanni[4]

[1]Key Laboratory of Tectonics and Petroleum Resources, Ministry of Education, China University of Geosciences, Wuhan, China, [2]Shenzhen Branch of the China National Offshore Oil Corporation, Shenzhen, China, [3]Fault Analysis Group, UCD School of Earth Sciences, University College Dublin, Dublin, Ireland, [4]DiSTAR, Università Degli Studi di Napoli "Federico II", Naples, Italy

Key Points:

- A first imaged metamorphic core complex (MCC) in the proximal northern South China Sea rifted margin and its 3-D structure is described
- Visual evidence for the gradual migration of the brittle-ductile transition and rolling hinge during the rolling-hinge evolution of a MCC
- The origin of the MCC was favored by a pre-existing midcrustal ductile layer and basement structures within the upper crust

Correspondence to:
Q. Ye,
qingye@cug.edu.cn

Citation:
Ye, Q., Mei, L., Jiang, D., Xu, X., Delogkos, E., Zhang, L., & Camanni, G. (2022). 3-D structure and development of a metamorphic core complex in the northern South China Sea rifted margin. *Journal of Geophysical Research: Solid Earth*, *127*, e2021JB022595. https://doi.org/10.1029/2021JB022595

Received 15 JUN 2021
Accepted 9 FEB 2022

Author Contributions:
Project Administration: Xinming Xu, Lili Zhang
Resources: Dapeng Jiang
Supervision: Lianfu Mei
Writing – review & editing: Efstratios Delogkos, Giovanni Camanni

Abstract The 3-D structure of continental metamorphic core complexes (MCCs) and their coevolution along with the associated extensional detachments are still not well understood. In this study, analysis of a newly acquired high-resolution 3-D seismic reflection volume reveals for the first time a well-imaged MCC in the proximal northern South China Sea (SCS) rifted margin, the Kaiping MCC (KP MCC). These data provide a 3-D view of the KP MCC and the associated KP detachment fault. The KP MCC is characterized by ascend of ductile midcrustal materials, and it is partially exhumed in the KP9 High. The KP detachment fault displays a domed low-angle geometry, and is characterized by pronounced NS-plunging corrugations, among which two megacorrugations of tens of kilometers are revealed. Evidence show that the KP MCC developed according to the classical rolling-hinge model. A group of secondary normal faults and fractures, which are parallel to the axis of the KP MCC and offset the KP detachment surface at the crest of the MCC, developed in response to inelastic bending during progressive warping of the footwall. The migration of the domal seismic reflection layers provides a visual evidence for the kinematic process of the rolling-hinge activity, during which the brittle-ductile transition and the rolling hinge gradually migrate as the detachment fault slips. The origin of the KP MCC in the northern SCS margin is suggested to have been favored by the existence of a pre-existing midcrustal ductile layer and basement structures within the upper brittle crust.

Plain Language Summary A metamorphic core complex (MCC) is an exposure of deep crust associated with extensional processes. Current understanding on MCCs is mainly derived from outcrop and geomorphic studies that only allow their exhumed part to be observed. A newly acquired 3-D seismic reflection volume reveals a well-imaged MCC, the Kaiping MCC (KP MCC), in the proximal northern South China Sea (SCS) rifted margin, permitting, for the first time, a detailed 3-D examination of the MCC structure and its associated detachment fault. In this study, we present the 3-D structure of the KP MCC, the geometry and kinematics of the associated KP detachment fault, and then we discuss the development and origin of the KP MCC. We propose that the KP MCC developed according to the rolling-hinge model, with our data providing a visual evidence for the kinematic processes during which the brittle-ductile transition and the rolling hinge gradually migrate as the detachment fault slips. We suggest that the origin of the KP MCC is favored by the existence of a pre-existing midcrustal ductile layer and basement structures within the upper crust. Our study not only have implication for the SCS rifting but also advance understanding on the development and origin of MCCs.

1. Introduction

A metamorphic core complex (MCC) is a domed structure that results from the process of lithospheric extension and subsequent isostatic readjustment, during which process, the brittle upper crust breaks and is displaced along an extensional detachment fault, while ductile crustal materials (or even upper mantle) ascend from deeper levels and become exhumed in the footwall of the detachment fault (e.g., Brun et al., 2018; Ring, 2014; Whitney et al., 2013). The extensional detachment that bounds the MCC on its top typically displays a low-angle (<30°), domed morphology and soles into the deep ductile crustal layer, although it is usually considered to initiate within the brittle upper crust at steeper angles (e.g., Little et al., 2019; Mizera et al., 2019; Webber et al., 2020). The detachment fault finally places the upper crustal rocks and the low-grade or unmetamorphosed sedimentary sequences in the hanging-wall against the metamorphic or plutonic rocks exhumed from the brittle-ductile

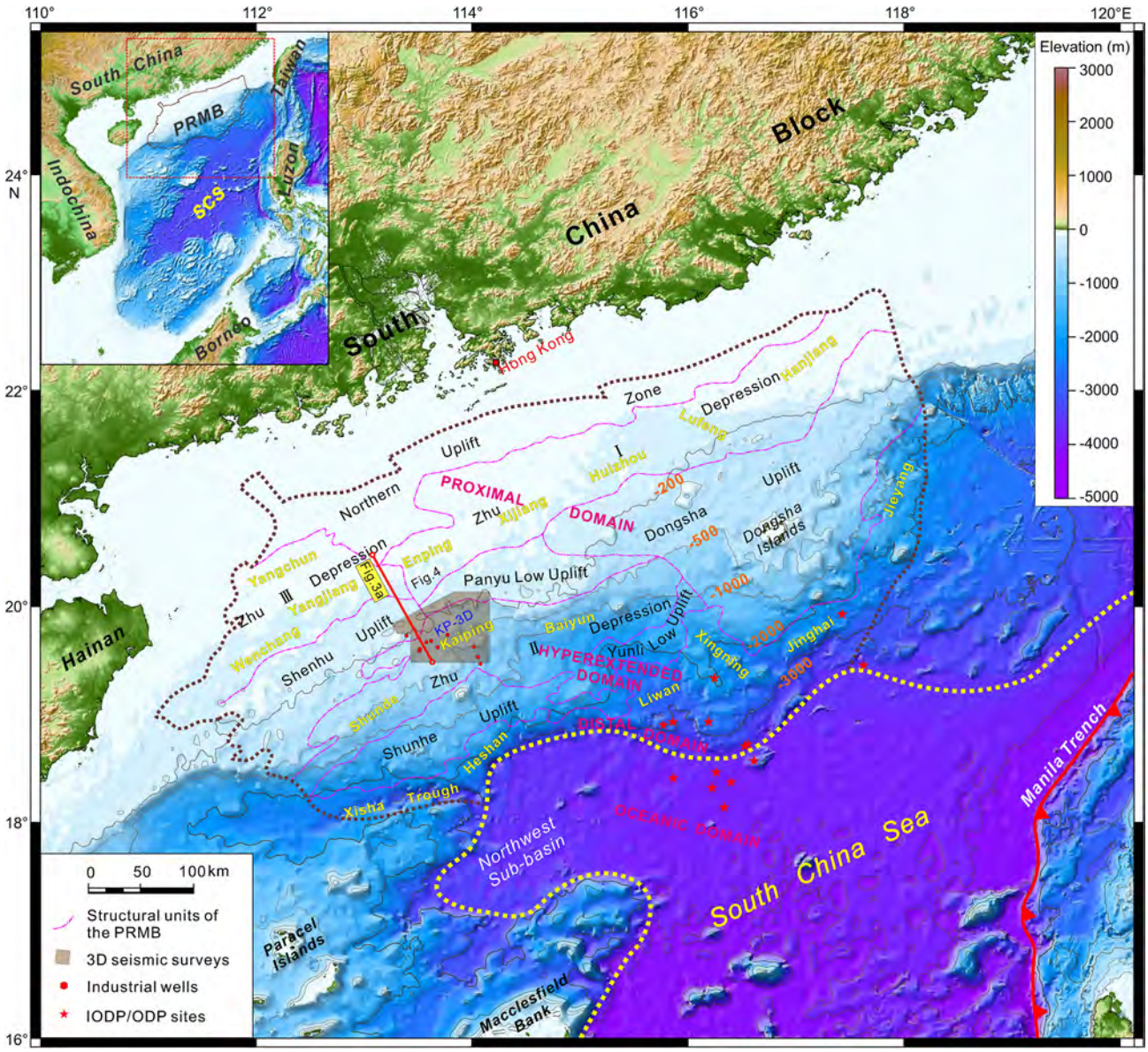

Figure 1. Bathymetric map of the northern South China Sea rifted margin showing structural units of the Pearl River Mouth Basin (PRMB). Location of the Kaiping Sag area and the datasets used in this study are marked. SCS—South China Sea.

transition in the footwall (Platt et al., 2015). Since their first identification around 1980 (Armstrong, 1982; Coney, 1980), MCCs are considered to be of high research value as they provide a "window" for investigating the mechanics and rheology of deep crustal levels (Platt et al., 2015).

While MCCs and their associated low-angle detachment faults are now widely recognized, some key questions regarding continental MCCs still remain enigmatic. To the best of our knowledge, although four decades have passed since their first identification, almost all the existing studies on continental MCCs are based on outcrops and geomorphic data, that have the implicit limitation of mostly allowing the exhumed and exposed part of MCCs to be examined. Therefore, the 3-D structure of a MCC and its associated detachment fault, and the kinematic processes of the deeper crust within the domed core of a MCC are aspects that have been less investigated often due to the lack of adequate data sets.

In this paper, we reveal for the first time a MCC developed in a previously less-studied area on the proximal domain of the northern South China Sea (SCS) rifted margin (Figure 1), and we investigate its structure by the

means of interpretation and analysis of a newly acquired high-resolution 3-D seismic reflection volume. This data set allowed us to examine and advance our understanding on the 3-D structure and kinematics of MCCs and their associated detachments. This study also provides new insights into the initial lithospheric structure and its influence on the Cenozoic rifting processes in the northern SCS.

2. Geological Setting

2.1. Geological Background

The SCS is tectonically situated at the junction of the Eurasian, Pacific, and Indo-Australian Plates, and is the largest marginal sea in the western Pacific region. Its development is a result of the Cenozoic rifting and seafloor spreading on the margin of the South China Block. The continental rifting linked with the opening of the SCS was diachronous along the margin, and the onset of rifting still remains poorly dated, and possibly dates back to the beginning of the Cenozoic (e.g., Morley, 2016; Savva et al., 2014). The continental breakup and seafloor-spreading process of the SCS was also diachronous, from the Late Oligocene to Middle Miocene (~32–15.5 Ma) and earlier at the northeastern part (Briais et al., 1993; Li et al., 2014).

The study area of this paper is located within the Pearl River Mouth Basin (PRMB), which is the largest Cenozoic rift basin on the northern margin of the SCS (Figure 1). The PRMB is made up of roughly NE-SW trending, alternating structural highs and lows, and is comprised of a proximal, a hyper-extended, and a distal domain. Two main rifting phases were recorded in the PRMB in relation to the opening of the SCS, an initial one characterized by NNW-SSE extension in the early to middle Eocene, and a late one with nearly N-S extension from the Late Eocene to the early Oligocene (Ge et al., 2020; Ye, Mei, Shi, Shu et al., 2018; Ye et al., 2020; Zhu et al., 2016). The syn-rift stratigraphic units associated with these two rifting phases are separated by three major horizons: the Tg, T80, and T70. The Tg is the rift-onset unconformity, which corresponds to a regional unconformity between Mesozoic and Cenozoic throughout the SCS area. The T80 is a basin-wide unconformity and represents the boundary between the syn-rift 1 and the syn-rift 2 units. The T70 is another basin-wide unconformity that corresponds to the breakup time of the SCS and usually is interpreted to mark the end of the syn-rift stage.

2.2. Location and Structure the Kaiping Sag

In detail, the study area embraces the Kaiping (KP) Sag, which is a part of the Zhu II Depression, one of the structural lows within the PRMB (Figure 1). The KP Sag is located on the proximal domain of the rifted margin, which has a crustal thickness of around 20–25 km (Yang et al., 2018; Zhou et al., 2018). Compared with the Baiyun Sag to its east (e.g., Zhou et al., 2018) and the Enping Sag to its north (Ye, Mei, Shi, Shu et al., 2018), the KP Sag is less studied and reported since it was not a preferred region for oil and gas exploration in the past. The KP Sag consists, in turn, of several subordinate subsags and internal highs. These subsags are: the Central Subsag, Eastern Subsag, Northeastern Subsag, Western Subsag, and the Southwestern Subsag (Figure 2a). The maximum depth of base rift surface is ca. 4.6 s TWT (ca. 8.4 km), located in the Central Subsag. The internal highs include the KP9, KP10, KP11, and KP6 (Figure 2a).

3. Data Set and Methods

The KP Sag is entirely covered by a new integrated 3-D seismic reflection volume, with an extent of 5400 km^2, which was acquired by the China National Offshore Oil Corporation (CNOOC) Shenzhen Branch. This seismic volume has a bin size of 12.5 × 12.5 m, and a vertical resolution of ca. 20m. The seismic data recorded to ca. 8s two-way travel time (TWT), above the Moho location which is usually located at ca. 9s TWT in adjacent regions within this domain of the rifted margin. Ten industrial exploration wells were drilled within the survey area and were tied to assist the seismic interpretation. Seismic interpretation was conducted using a standard industrial process in GeoFrame and Petrel Software. Time-depth conversion for the sedimentary covers within Cenozoic rift basin used in this paper was performed by using a best-fit second-order polynomial derived from the 10 boreholes, $D = 0.000251*T2 + 0.646808*T$ (D-depth/m, T-TWT/ms, $R^2 = 0.997446$); and for depth calculation within the crust below the Tg surface, we use 6.5 km/s as the average seismic velocity for the whole crust, which was suggested by Zhou (2018) for the northern SCS rifted margin, and the calculation error was considered to be less than 0.1 km per second.

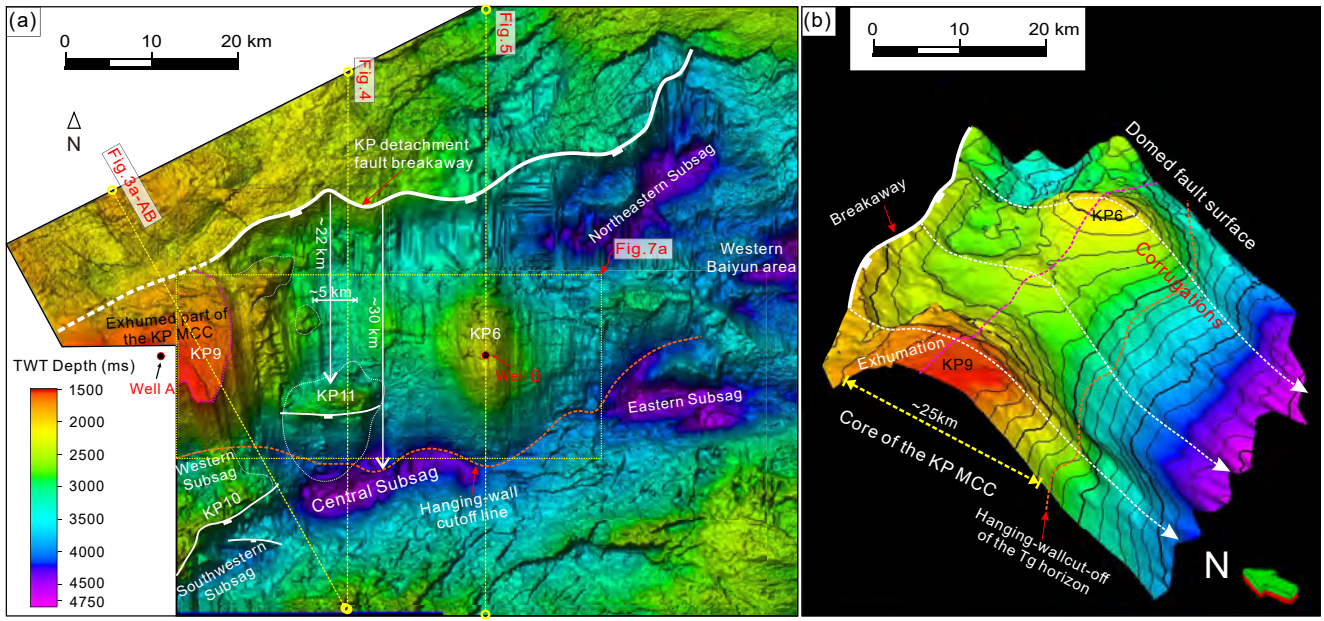

Figure 2. (a) Two-way time structural map of the base rift surface (i.e., Tg) of the Kaiping (KP) Sag illustrating the general rift configuration. (b) Morphology of the domed and corrugated KP detachment fault surface. The pink dotted line indicates the hinge of the KP metamorphic core complex.

4. Results

4.1. Imaging of a Reflective Ductile Midcrustal Layer and the Kaiping MCC

The Cenozoic KP Sag developed above a large-scale dome structure (Figures 2–5), which displays an E-W trending long axis within the survey area from the KP9 High to the KP6 High, extending more than 50 km (Figure 2a). This dome structure has a variable amplitude and width along its strike that generally is wider (~25 km wide) and higher at the western part and gradually decreases eastwards, and then disappears.

From the seismic sections across the KP Sag, a layered crust can be clearly observed (Figures 3–5). The upper crust layer is characterized by relatively weak and chaotic reflection, with pervasive reflectors caused by pre-existing brittle fault structures, which are similar to those described in adjacent regions in the proximal domain of the rifted margin (Ye, Mei, Shi, Camanni et al., 2018; Ye, Mei, Shi, Shu et al., 2018; Ye et al., 2020). Important for this paper, a highly reflective midcrustal layer, which combines a group of high amplitude continuous reflectors, was detected from the 3-D seismic reflection survey. This highly reflective midcrustal layer shows distinct seismic characteristics from the upper crust, as well as the lower crust which also shows less reflective and continuous features. Based on integrated analysis on the deep seismic reflection profiling of the continental crust worldwide, Klemperer (1987) suggested that the highly reflective zone is generally developed at temperatures higher than 300°–400°C; and it has widely been related to the ductile banding below the BDT (brittle-ductile transition) and the top of it is called K horizon (Brun & Gutscher, 1992; Carcione & Poletto, 2013; Gianelli et al., 1997; Liotta & Ranalli, 1999; Meissner & Strehlau, 1982). In this study, the pre-existing brittle faults within the upper-crust basement generally sole into this reflective midcrustal layer (Figure 3), which also indicates the ductile behavior of this highly reflective mid-crustal layer. The highly reflective midcrustal layer has a relatively steady thickness of ca. 3–6 km, and thickens within the core of the dome structure (Figures 3–5), suggesting a ductile flow of it toward the core of the dome structure during its uplift.

By analyzing the seismic line shown in Figure 3a in its entire length, it can be noticed that the highly-reflective mid-crustal layer can be continuously tracked from the western Enping Sag, through the Shenhu Uplift to the KP Sag. It is relatively flat around ca 6–7s TWT (ca ~10–17 km) in the western Enping Sag and the Shenhu Uplift, while it gradually ascends southward to ca. 1.7s TWT (~1.8 km) in the KP9 High of the KP Sag, which causes the dome structure within the KP Sag. Moreover, this midcrustal layer was exhumed and unroofed at the KP9 High of the dome structure, leading to the development of the flat topography of the KP9 High as observed on the TWT structure map of the Tg Horizon (Figure 2a). The ductile mid-crustal layer was not exhumed in the

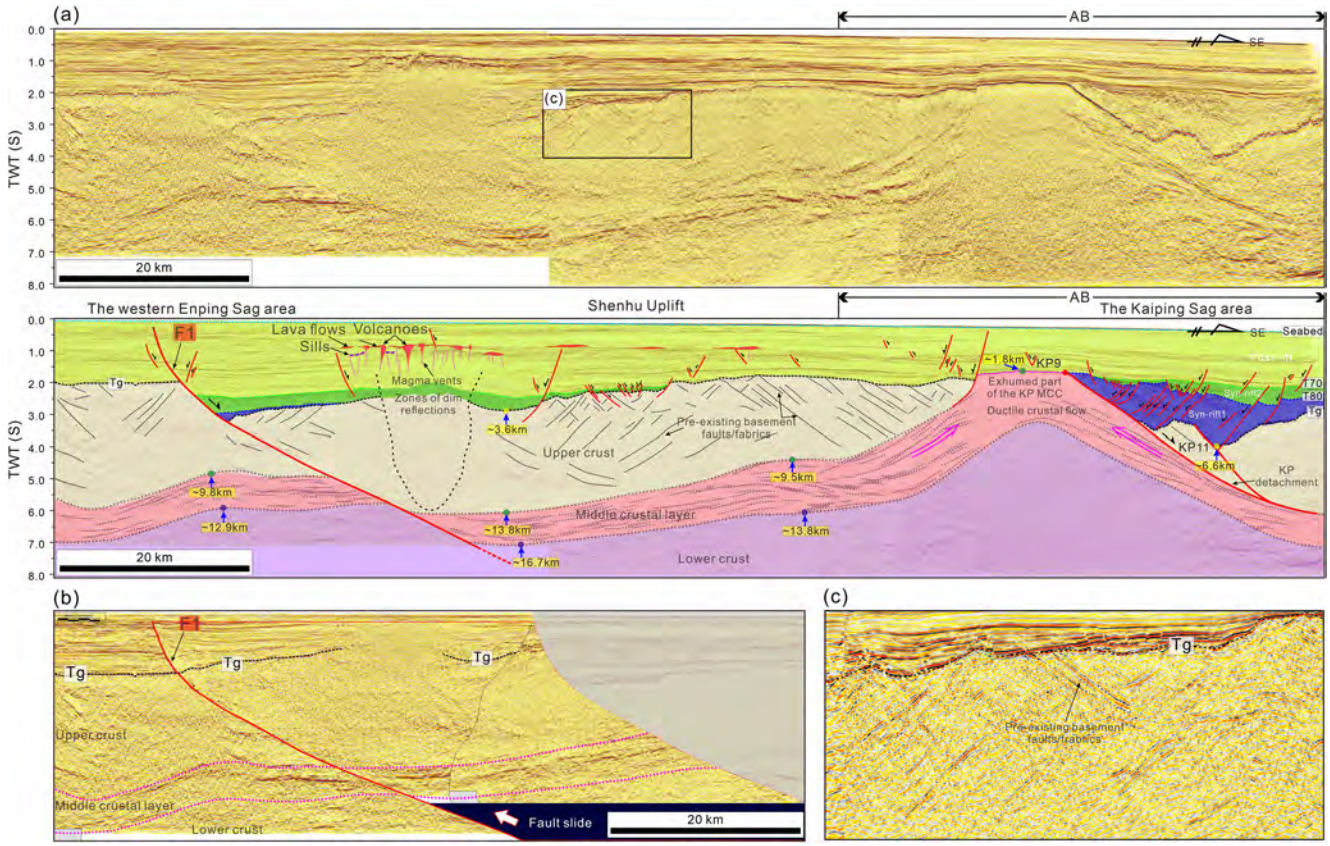

Figure 3. (a) A composite 3-D seismic section across the western Enping Sag, the Shenhu Uplift and the KP9 High of the KP Sag in the northern South China Sea rifted margin (see Figure 1 for location, and the location of the AB segment of this section is also shown in Figure 2a). (b) Displacement restoration of the F1 fault using the Fault Slide tool in Geoframe Software. Notice that when the fault displacement at the Tg Horizon is restored, the faulted reflective middle crustal layer also becomes continuous, indicating that the reflective middle crustal layer existed prior to slip on this fault. (c) Expanded view of pre-existing basement faults/fabrics within the brittle upper-crust basement.

eastern parts where it only reached the base of the Cenozoic rift basin, meanwhile, the upper crust broke and was displaced along the extensional detachment fault, leading to the juxtaposition of the Cenozoic syn-rift sedimentary sequences against the reflective midcrustal layer (Figures 4 and 5).

Due to the distinctive seismic reflection characteristics of the upper and middle crust, their boundary can be interpreted in seismic lines (Figures 3–5), and the TWT depth map for the top boundary of the reflective mid-crustal layer can be identified (Figure 6a). Our mapping shows that the morphology of the dome structure correlates well to the undulation of the deep-seated mid-crustal layer (Figure 6b). Besides, this dome structure shows high positive gravity anomalies with oval geometries, which are interpreted to indicate the uplift of high-density rocks from the middle to lower continental crust, with the KP9 and KP6 Highs presenting two extreme points on this map (Figure 6c).

All the aforementioned features of the large-scale dome structure within the KP Sag described above conform to the definition of a MCC, as described in the introductory section, and is named the KP MCC in this paper. This statement is also supported by the two industrial wells that have drilled into the basement, the Well A and B, located at the KP9 and KP6 Highs respectively (see locations in Figures 2a and 6). The basement rocks revealed by the Well A and Well B are metaquartzite and metamorphic volcanic rock, respectively. The Cenozoic syn-rift 1 units above the domal core of the KP MCC are truncated by the T80 horizon and show a clear angular unconformity (Figures 3–5 and 7), while the syn-rift 2 units overlap on it, indicating that the uplift of KP MCC terminated at the end of the syn-rift 1 stage. This MCC seems to extend westwards, further of the area covered by the 3-D seismic reflection survey, and changes its trend to SW-NE (Figure 6).

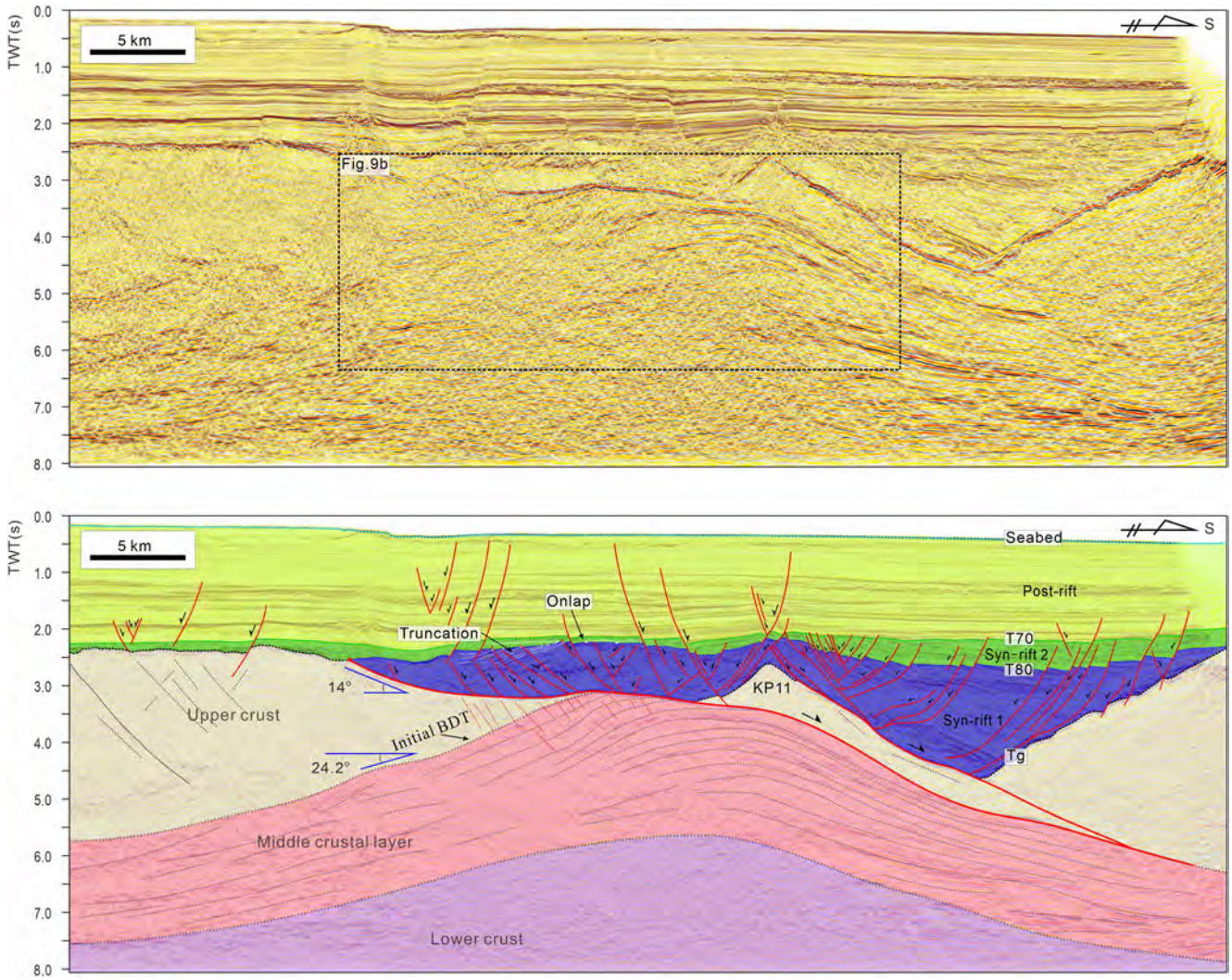

Figure 4. Uninterpreted and interpreted seismic section across the KP11 Block within the KP Sag mainly showing the structure of the KP metamorphic core complex in the western part of the study area (see Figure 2a for location), BDT——brittle-ductile transition.

4.2. Geometric and Kinematic Characteristics of the Kaiping Detachment Fault

Following the interpretations and results from the previous section, the Cenozoic syn-rift deposition of the KP Sag is mainly bounded in the north by a detachment fault, named the KP detachment fault. The KP detachment fault is roughly ENE-striking and the corresponding depocenter displays the same ENE trend (Figure 2a). The detachment fault surface has a domed low-angle geometry, which bounds the KP metamorphic core complex at its top and soles into the reflective mid-crustal ductile layer (Figures 2b, 3a, 4 and 5). The current dip angles of the KP detachment at its upper part, calculated based on the seismic sections presented in Figures 4 and 5, are ca. 14° and 11.3° respectively. The max fault heave of the KP detachment fault (i.e., the extension amount) on the Tg horizon is ca. 30 km at the center of the Central Subsag that can be directly measured on map (Figure 2a), where the corresponding fault throw is as large as 5 km. The KP detachment fault is truncated at the KP9 High since the KP MCC is exhumed at this location (Figures 2b and 3a).

The KP detachment fault surface displays pronounced corrugations (Figures 2 and 7), a common feature in both continental and oceanic MCCs globally, although their origin remains disputed (Escartín et al., 2017; Mizera et al., 2019; Parnell-Turner et al., 2018; Singleton, 2013). Such corrugations on the KP detachment surface are defined by multiscale ridges and grooves (Figure 7). Among them, the KP6 and KP9 are the peaks of two megacorrugations, with wavelengths in scale of tens of kilometers and amplitudes of thousands of meters, which

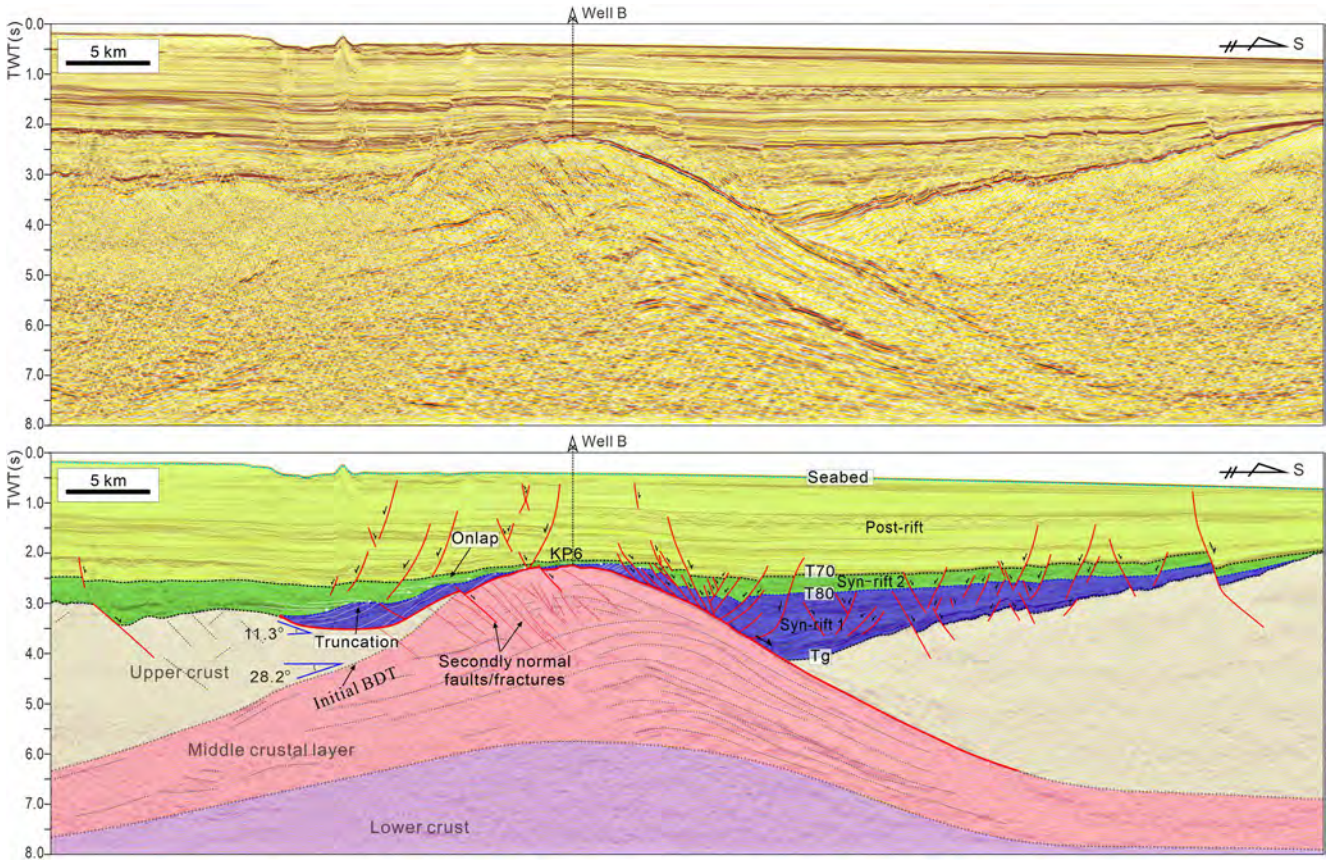

Figure 5. Uninterpreted and interpreted seismic section across the KP6 High within the KP Sag showing the structure of the KP metamorphic core complex and the associated detachment fault (see Figure 2a for location). Notice that some portions of the syn-rift 1 sequence were abandoned on the detachment fault in the northern flank of the domal core.

also extend below the hanging wall cut-off of the Tg horizon (Figure 2b). These detachment corrugations display a consistent plunge with a nearly N-S trend, which is consistent with those described for other detachment faults mapped in the northern Enping Sag (Ye, Mei, Shi, Shu et al., 2018) and the southeastern Liwan Sag in the hyper-extended domain (Deng et al., 2020). Corrugations observed on major slip surfaces are considered an important indicator of fault slip direction (Edwards et al., 2018; Lymer et al., 2019; Parnell-Turner et al., 2018; Resor & Meer, 2009), and, therefore, they suggest that the extension direction along the KP detachment fault is top down to the south.

The KP10 and KP11 are two large basement blocks overlying the corrugated KP detachment fault surface (Figure 2a). These basement blocks are common features of low-angle detachments and MCCs that can slip for large distances on the detachment surface and are termed rider blocks (e.g., Choi & Buck, 2012; Webber et al., 2020; Whitney et al., 2013). The KP11 block, for example, slips along a ca. 5 km wide groove for a distance of ca. 22 km away from the fault breakaway (Figure 2a). Furthermore, it is worth noting that the corrugations on the KP11 hanging-wall block-bounding fault plane do not just align with the corrugations observed on the basal KP detachment fault surface, but accurately match ridge and trough with corrugations on the KP detachment fault (Figure 7a). Similar observation was recently documented in a detachment fault at the Galicia rifted margin, west of Spain, which was considered as evidence that the block-bounding fault developed later and nucleated on the basal detachment fault then propagated upwards, and then both surfaces have slipped together (Lymer et al., 2019).

As shown from the enlarged map of the base rift surface in Figure 7a and the seismic section in Figure 5, the KP detachment fault and its associated corrugations were orthogonally crosscut by an array of secondary ca. EW-striking, small-displacement normal faults developed above the domal core of the MCC. This feature of the

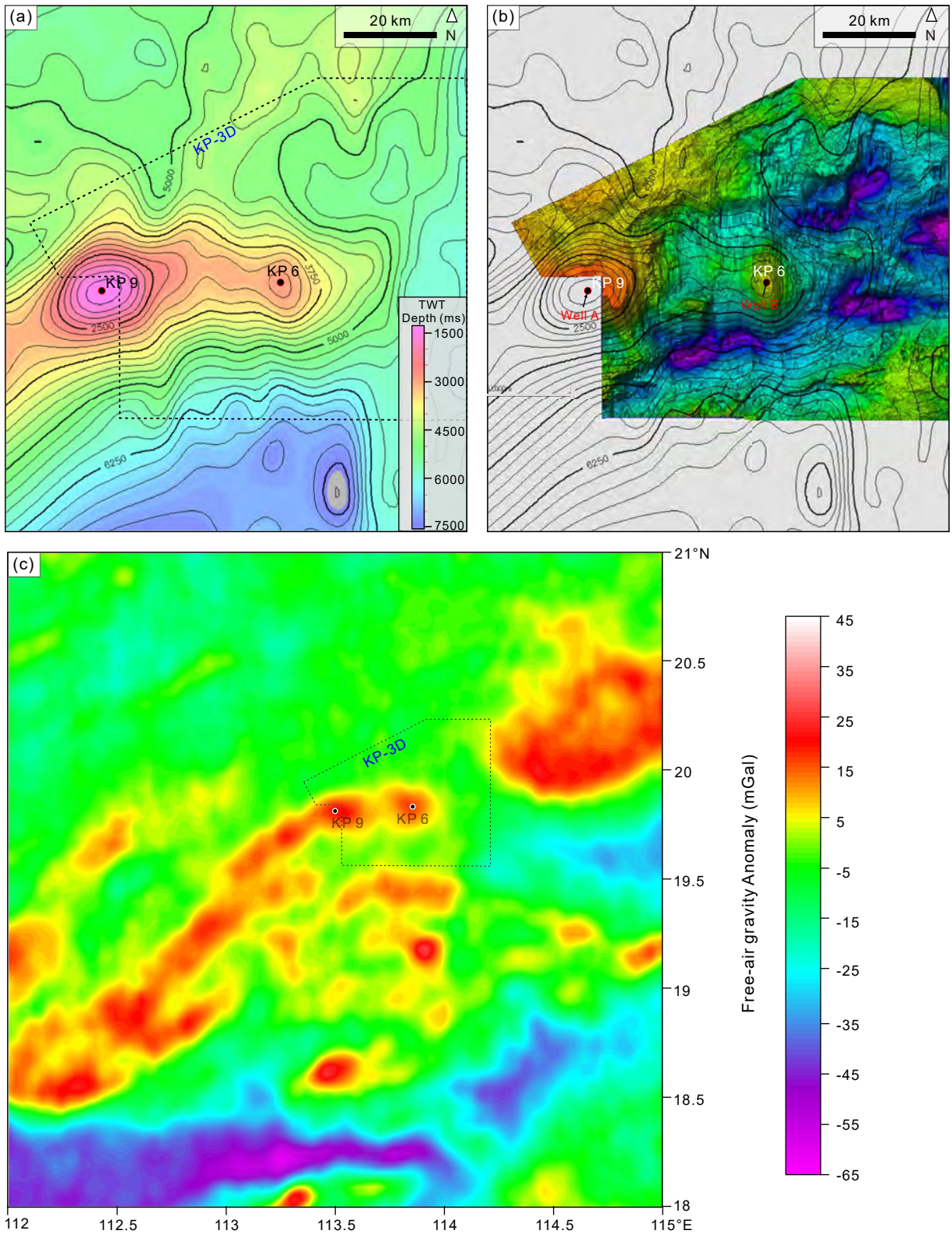

Figure 6. (a) Two-way travel time (TWT) depth map for the top surface of the reflective midcrustal layer; (b) Contours in Figure 6a superposed on the TWT structure map of the base rift surface in Figure 2a, showing the correlation between the uplifted midcrustal layer with the morphology of the Kaiping metamorphic core complex as defined by the elevation of the basement Tg surface; (c) Satellite-derived one-minute free-air gravity anomaly map around the study area. The gravity data were extracted from the global marine gravity model V29.1 produced by Sandwell et al. (2014).

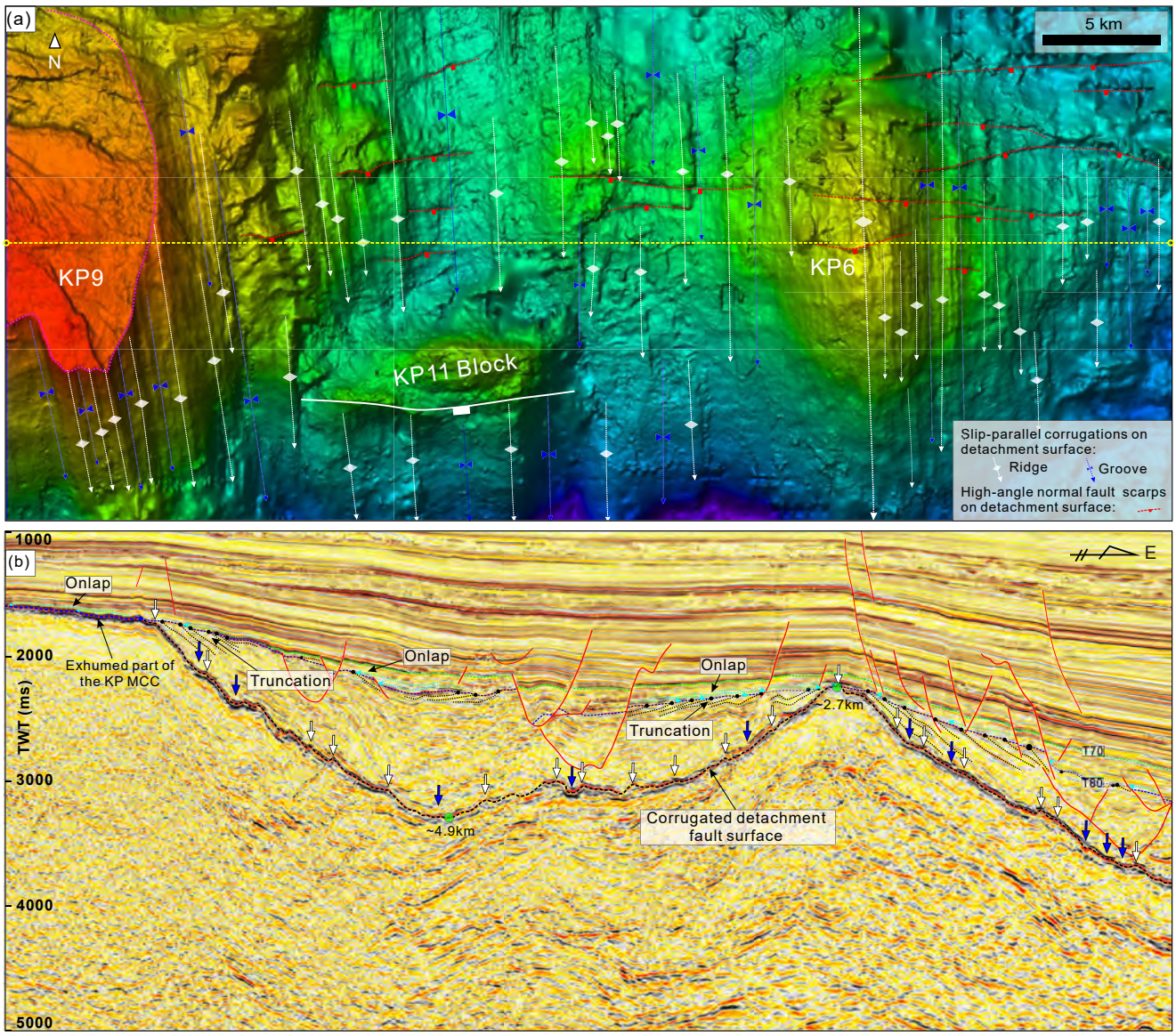

Figure 7. (a) Enlarged map of the time-structure map of the base rift surface (see Figure 2a for location) showing detailed view of fault corrugations and secondary normal faults on the Kaiping (KP) detachment faut surface, acquired by 1 × 1 dense of seismic interpretation. The corrugations on the KP11 block-bounding fault plane align with corrugations observed on the basal KP detachment fault surface, and accurately match ridge and trough. (b) Seismic section along the axis of the KP metamorphic core complex showing the detachment fault corrugations and the truncation of the syn-rift 1 strata at the T80 horizon and the syn-rift 2 sequence onlapped on it.

detachment surface above the domal core of the MCC is similar to many detachment surfaces documented in both oceanic and continental MCCs (Axen et al., 1995; Hayman et al., 2011; Karson et al., 2006; Mizera et al., 2019; Spencer, 2011; Tucholke et al., 1998, 2008).

5. Discussion

5.1. Model for the Development of the Kaiping Metamorphic Core Complex

The development and evolution of MCCs and associated detachments have been typically described by two prominent models (Figure 8) (e.g., Little et al., 2019; Mizera et al., 2019; Platt et al., 2015). (a) The rolling-hinge model: normal fault initiates at steep dip and progressively flattens with slip as a result of unloading-related back tilting of the exhumed fault, while remaining active at depth (e.g., Axen & Hartley, 1997; Buck, 1988; Webber

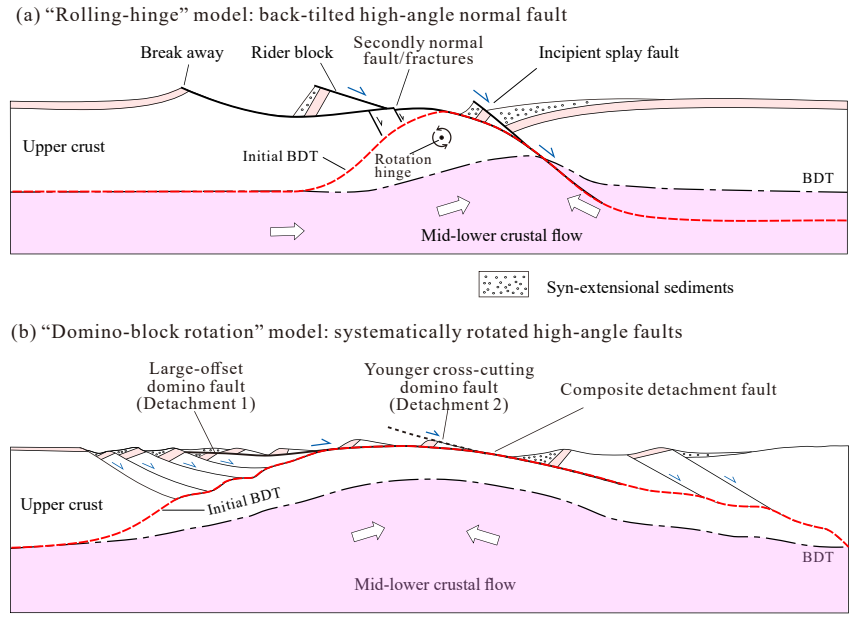

Figure 8. Two prominent models for the evolution of metamorphic core complexes and the associated large-displacement low-angle detachment faults (modified from Little et al., 2019; Mizera et al., 2019), BDT——Brittle-ductile transition.

et al., 2020; Wernicke & Axen, 1988). (b) The domino-block rotation model: an array of normal faults form at high angles over a distributed region and simultaneously begin to rotate to shallower angles. Low-angle faults eventually may be crosscut by younger high-angle normal faults which will also progressively rotate to shallower dips. The final geometry may include a composition of different-aged fault segments that form a composite detachment fault, resembling a single-detachment fault (Gans & Gentry, 2016).

This study provides strong evidence that the KP MCC and the associated detachment fault have evolved through the classical rolling-hinge model. First, the KP detachment fault is a single, continuous, large-offset fault, in contrast to the composite detachment fault expected by the domino-block rotation model (Gans & Gentry, 2016; Mizera et al., 2019), and it is also associated with splay faults and corresponding rider blocks (the KP10 and KP11 blocks). Furthermore, the bounding fault of the KP10 rider block is indicated to develop later than the basal detachment fault (see Section 4.2), reflecting sequential splay faulting in the upper plate, which is also a prominent feature of the rolling-hinge model. Second, the back-tilting of the syn-rift 1 sequence at the hanging wall of the low-angle part of the detachment fault in the northern flank of the domal core (Figures 4 and 5) indicates that this low-angle part of the detachment surface has undergone syn-tectonic rotation, and it would be expected to have a steeper dip angle at earlier time. This process is consistent with the rolling-hinge model, in which case, due to the isostatic rebound and the warping of the unloaded footwall, the shallower part of an originally moderate to steeply dipping fault progressively tilts back to lower dips and the footwall back-warps into an abandoned, domal structure (Figure 8a). In addition, due to that the rotation of the fault is achieved by gradual warping of the footwall, the footwall that behaves as a flexed elastic beam may partially fail in response to bending stresses (Figure 8a) (Mizera et al., 2019). It is therefore suggested that the development of the secondary EW-striking normal faults that cut and offset the KP detachment surface above the domal core as presented in Figures 5 and 7a is probably due to the inelastic bending of the footwall and the fault surface during the rolling-hinge activity. Similar structures have been also observed in other MCCs (Axen et al., 1995; Hayman et al., 2011; Karson et al., 2006; Mizera et al., 2019; Spencer, 2011; Tucholke et al., 1998, 2008). Therefore, they are expected to be parallel to the long axis of the MCC and locally distributed on the crest of the dome where the maximum strain should have been concentrated during the rolling-hinge process.

5.2. Implications for the Kinematic Processes of the Rolling-Hinge Activity

Based on lithosphere-scale numerical modeling of metamorphic core complex development, Tirel et al. (2008) and Brun et al. (2018) suggested that during extension and coeval rising of the core during the rolling-hinge

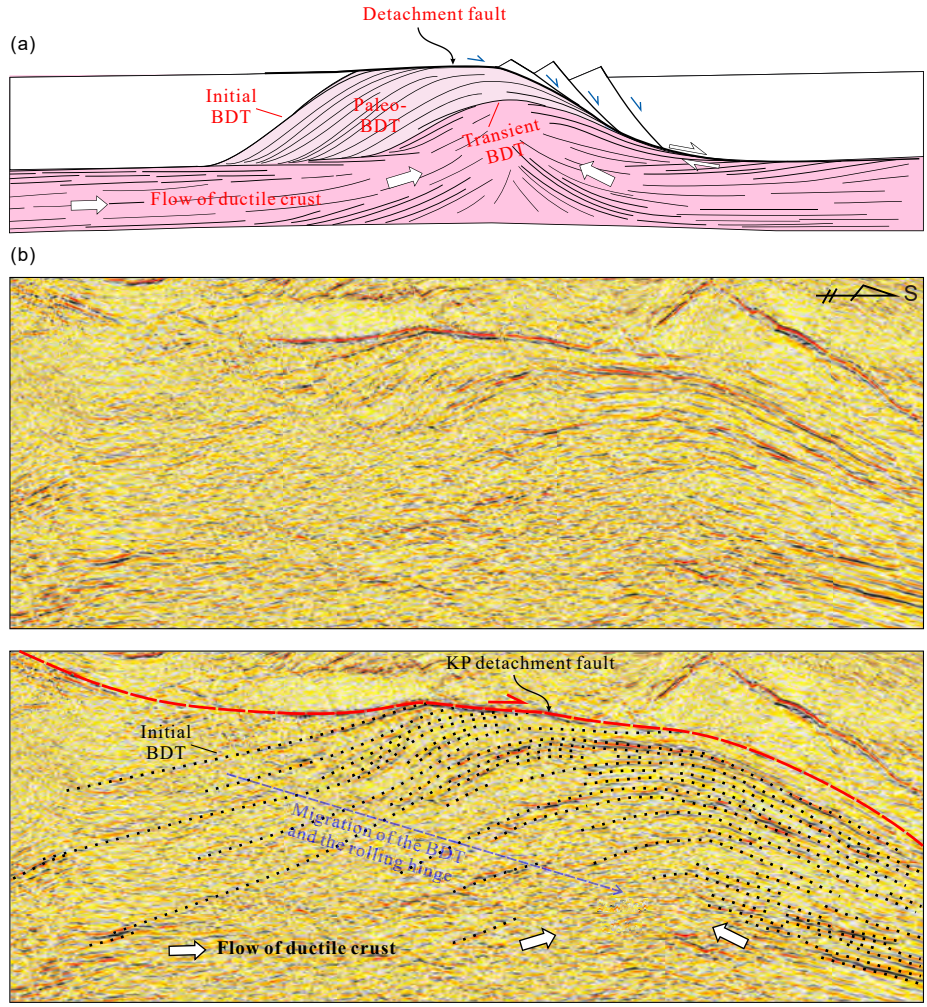

Figure 9. (a) Conceptual model illustrating the structure of the ductile part of the core complex as defined by foliation trajectories that is suggested by numerical modeling (modified from Brun et al., 2018). (b) Uninterpreted and interpreted seismic section showing the seismic reflection feature within the core of the Kaiping metamorphic core complex (MCC). Notice the migration of the domed seismic reflectors from north to south, indicating the migration of the brittle-ductile transition and the rolling hinge duing the growth of the MCC (see Figure 4 for location).

process, the ductile rocks progressively cool and cross the transient brittle-ductile transition (BDT), then become brittle and part of the footwall brittle crust; their results suggested that the growth of the core complex manifests as asymmetrical, and the active part of the core complex progressively migrates together with the detachment (Figures 9a and 10). However, this significant understanding on the rolling-hinge development of MCC has not yet been well supported by direct evidence from natural examples.

Important for this study, we consider that the 3-D seismic reflection volume provides unprecedented evidence of this process. The data indicate that the domed seismic reflectors within the core of the KP MCC gradually migrated southwards into deeper levels (Figure 9b, also see Figures 4 and 5). We interpreted that these domed seismic reflectors potentially represent the paleo-BDTs, with their southward migration providing evidence for the gradual migration of the transient BTD and the rolling hinge as the detachment fault accumulates slip during the rolling-hinge evolution of a MCC (Axen & Hartley, 1997; Axen et al., 1995; Mizera et al., 2019). The upper part of the reflective core is suggested to be the earlier ductile crustal rocks that has become brittle, and this could be the reason why some of the secondary high-angle normal faults and fractures extend down to this level (Figures 5 and 10).

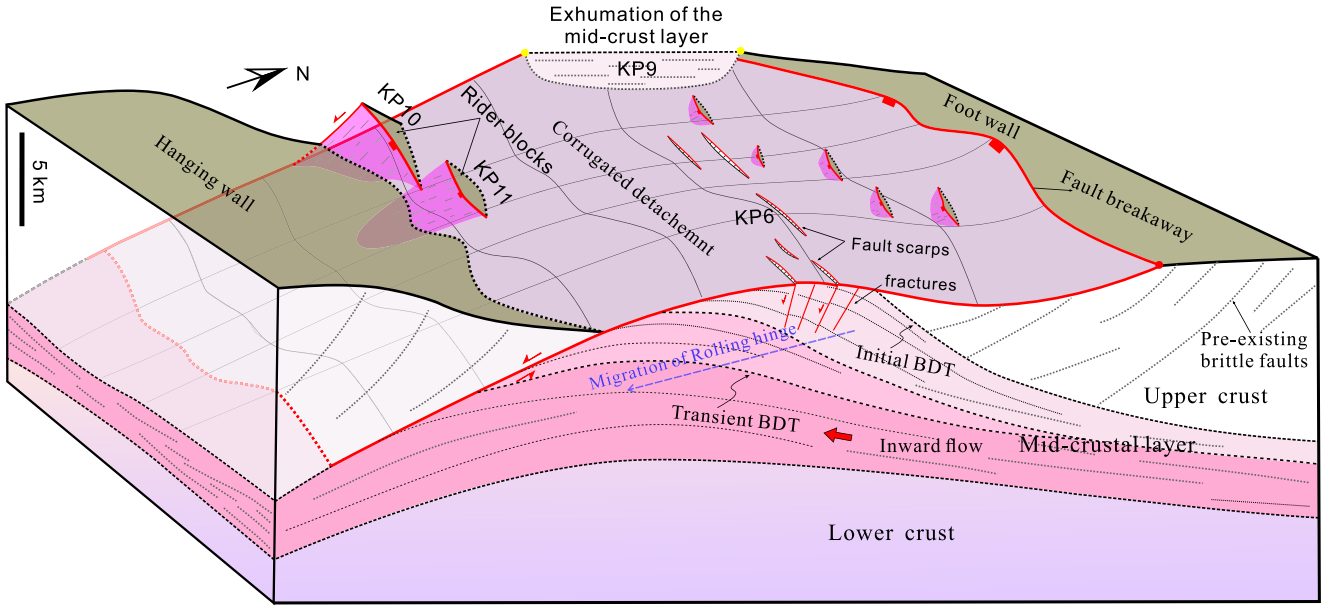

Figure 10. Three-dimensional block diagram illustrating the Kaiping (KP) metamorphic core complex (MCC) and the corrugated KP detachment fault. The development of the KP MCC is closely related to the syn-rift ascending and partial exhumation of a reflective midcrustal ductile layer, and has evolved though a rolling-hinge process. The detachment surface is prominently corrugated, and was overlain by some rider blocks. The crest of the domal core was crosscut by some secondary high-angle faults and fractures that were formed in response to progressive bending of the footwall and the detachment surface. During the rolling-hinge process, the early ductile crustal rocks progressively cool and cross the transient brittle-ductile transition, and eventually become part of the footwall brittle crust, while the active part of the core complex and the rolling hinge progressively migrate together with the detachment zone.

5.3. The Original Dip Angle of the KP Detachment Fault

An important factor of the rolling-hinge evolution of a MCC is the estimation of the original dip angle of the detachment fault, in order to calculate the magnitude of flexural back rotation in the footwall. This estimation is usually carried out by geometric reconstruction under the constrain of pre-rift sub-horizontal markers in the footwall (Axen, 2004; Lecomte et al., 2010; Smith et al., 2007), and assuming that extension was accompanied by rigid-body rotation (Westaway & Kusznir, 1993). The fault cutoff angles of the syntectonic strata in the hanging wall of the detachment fault were also used in some studies to estimate the original fault dip angle (Mizera et al., 2019; Webber et al., 2020). However, we think that the latter method has some theoretical problems since the fault cutoff angles of the syntectonic sequences are not only influenced by the rolling of the footwall but also by the flexure of the hanging wall, resulting in inaccurate estimation of the original fault dip angle at the ground surface.

In this study area, there are no prerift sedimentary layers at the footwall of the KP detachment fault that can be used as markers to estimate the original fault dip angle. Therefore, we suggest that the geometry of the initial BDT (brittle-ductile transition) can be used as a geological marker assuming its near horizontal primary dip; this method was also used in estimating the initial dip angle of a low-angle normal fault at the Enping Sag (Zhou et al., 2019). By calculating the rotation angle of the initial BDT and the current dip of the upper part of the detachment fault, the initial dip angle of the KP detachment fault can be roughly estimated (ca. 38.2° and 39.5° for the seismic sections in Figures 4 and 5, respectively), indicating that the currently low-angle KP detachment fault initiated at a moderate angle.

5.4. Origin of the KP Metamorphic Core Complex

The influence of the geodynamic settings on the development of MCCs has been not well constrained (Brun et al., 2018; Whitney et al., 2013). It is obvious that MCCs are not widespread in all extensional regions and can only be developed under special tectonic conditions. Although it was theoretically suggested by numerical modeling that their occurrence in continents and continental rifted margins is significantly influenced by the initial rheological anomaly of the lithosphere before extension and strain localization within the upper crust

during extension (e.g., reviewed by Brun et al., 2018; Whitney et al., 2013; Wu & Lavier, 2016), few studies have presented compelling geological evidence for this since it is hard to define the initial condition of the lithosphere that has been superposed by later extension process.

This study provides evidence that the mid-crustal ductile layer which is interpreted to contribute significantly to the development of the KP MCC has already existed before the initiation of the Cenozoic rifting in the northern SCS, rather than being induced by the change of thermal conditions or ductile shear during the Cenozoic rifting process. First, this reflective midcrustal ductile layer is not only locally distributed with in the KP Sag rifting zone, but also extends far northwards to the Shenhu Uplift zone where Cenozoic rifting does not take place or is less developed, instead of only post-rift units covering (Figure 3a). Second, the pervasive pre-existing faults within the brittle upper crust all sole out into the top of this reflective midcrust ductile layer, indicating their same pre-existing nature (Figure 3a). Third, in the northern part of the seismic section in Figure 3a, the reflective mid-crustal ductile layer was crosscut by a fault related to the Cenozoic rifting, that is, the F1 fault (Figure 3a), with a ca. 4 km normal offset, and well-developed postrift volcanism exactly above of this faulted portion of the reflective mid-crustal layer. It is interesting that restoration of the displacement of the F1 fault at the Tg Horizon shows that the previously faulted reflective middle crustal layer also becomes continuous (Figure 3b). This suggests an equal amount of displacement of the F1 fault at the Cenozoic rift base (i.e., Tg) and at the deeper reflective middle crustal layer, which potentially indicates that the seismic-imaged middle crustal layer existed before the Cenozoic rifting initiation, and was later crosscut by the rift-related F1 fault. This reflective mid-crustal ductile layer is very likely to correspond to a previously revealed mid-crustal low-velocity layer (LVL) that has been discovered sporadically both onshore and offshore SCS and is also considered to be ductile and reflective in teleseismic recordings, with a similar thickness of ca. 5 km and depth varying from 9 to 16 km (e.g., Huang et al., 2019; Zhao et al., 2006; Zhou et al., 2020). The origin of this LVL is still a controversial issue, that may be caused by fluids from dehydration of subducted slab and trapped in the midcrust or partial melting within the mid-crust (Zhao et al., 2006 and references therein; Zhou et al., 2020).

It was considered that MCCs are common in highly extended domains of both continental and oceanic lithosphere (e.g., Coney, 1980; Whitney et al., 2013). The KP Sag is situated on the proximal domain of the rifted margin with an average crustal thickness ca. 20–25 km and, structurally, it does not belong to the hyper-extended part of the rifted margin (Yang et al., 2018; Zhou et al., 2018). Hence, we suggest that the initial structure of the lithosphere which comprised a pre-existing midcrustal ductile layer, rather than the amount of crustal extension, have played the more determinant role for the origin of the KP MCC. The mid-crustal ductile layer may have acted as weak domains during the rifting process. Furthermore, recent studies indicated that the Cenozoic rifting structures in the proximal domain of the northern SCS rifted margin were significantly influenced by reactivation of pre-existing thrust faults within the upper-crustal basement (Ye et al., 2020, Ye, Mei, Shi, Camanni et al., 2018; Camanni & Ye, 2022). Especially in the Enping Sag area just on the north of the KP Sag area, clear pre-Cenozoic imbricate thrust system has been revealed within the basement (Ye, Mei, Shi, Shu et al., 2018; Ye, Mei, Shi, Camanni et al., 2018). In the KP Sag area in this study, some reflective basement faults and fabrics are also imaged (Figure 3c). We speculate that the KP Sag area has been also influenced by reactivation of pre-existing basement faults during the earlier rifting stage, which may have led to localized surface extension resulting in a relatively quick unloading of the footwall, triggering the ascent of the weak ductile mid-crustal material, hence favoring the development of the MCC in this domain of the rifted margin.

6. Conclusions

A newly collected high-resolution 3-D seismic volume reveals for the first time a well-imaged metamorphic core complex (MCC) in a previously less-studied area, the KP Sag, in the proximal domain of the northern South China Sea (SCS) rifted margin. The 3-D nature of the seismic reflection data provides an unprecedented 3-D view of the MCC and the associated detachment fault, allowing a detailed determination of the 3-D structure of MCCs and their co-evolution along with the associated detachment faults. Our study shows that:

1. The KP MCC is closely related to the doming and partial exhumation of a reflective mid-crustal ductile layer during the syn-rift 1 evolution of the KP Sag, which displays an E-W trending long axis and extends more than 50 km within the survey area. It has larger amplitude and width in the west, and gradually descends and disappears eastwards.

2. The associated KP detachment fault displays a domed low-angle geometry, with a rough ENE strike, that soles into the reflective mid-crustal ductile layer. The detachment fault surface is charactered by many NS-plunging corrugations, among which two megacorrugations are characterized by wavelengths in the scale of tens of kilometers and amplitudes of thousands of meters. The corrugations on the block-bounding fault plane align with the corrugations observed on the KP detachment fault surface, and accurately match ridges and troughs, indicating that the block-bounding fault propagated upwards from the basal detachment fault.
3. The KP MCC developed according to the classical rolling hinge model, and the currently low-angle KP detachment fault initiated at a moderate angle of ca. 39°. A group of secondary EW-striking normal faults and fractures cut the KP detachment surface on the crest of the MCC developed in response to stresses that accommodate inelastic bending during progressive warping of the footwall. The migration of the domed seismic reflectors within the core of KP MCC provides a visual evidence for the kinematic process of the rolling-hinge activity of MCCs, during which the BDT and the rolling hinge gradually migrate as the detachment fault slips.
4. The origin of the KP MCC in the northern SCS margin is suggested to have been favored by a pre-existing midcrustal ductile layer, as well as by the pre-existing basement structures within the brittle upper crust that may have led to the localized surface extension during the earlier rifting stage.

Data Availability Statement

The raw seismic data used in this study are private and hence only high-resolution images are provided, which are archived in Figshare repository (https://figshare.com/s/5ae4c08b8d14fe954282).

Acknowledgments
The authors want to thank an anonymous reviewer and an expert Associate Editor for their detailed reviews and the Editor, Isabelle Manighetti, for manuscript handling and constructive suggestions. The Shenzhen Branch of the China National Offshore Oil Corporation is thanked for providing seismic reflection data presented in this study. This study was financially supported by the Fundamental Research Funds for the Central Universities, China University of Geosciences (Wuhan) (No. 162301192684 & No. G1323520282) and the Major National Science and Technology Programs, China (No. 2016ZX05026-003-001). E. Delogkos is funded by the Irish Research Council under Grant No. GOIPD/2020/530.

References

Armstrong, R. L. (1982). Cordilleran metamorphic core complexes-from Arizona to southern Canada. *Annual Review of Earth and Planetary Sciences*, *10*(1), 129–154. https://doi.org/10.1146/annurev.ea.10.050182.001021

Axen, G. J. (2004). Mechanics of low-angle normal faults. In *Rheology and deformation of the lithosphere at continental margins* (pp. 46–91). Columbia University Press. https://doi.org/10.7312/karn12738-004

Axen, G. J., Bartley, J. M., & Selverstone, J. (1995). Structural expression of a rolling hinge in the footwall of the Brenner line normal fault, eastern Alps. *Tectonics*, *14*(6), 1380–1392. https://doi.org/10.1029/95tc02406

Axen, G. J., & Hartley, J. M. (1997). Field tests of rolling hinges: Existence, mechanical types, and implications for extensional tectonics. *Journal of Geophysical Research*, *102*(B9), 20515–20537. https://doi.org/10.1029/97jb01355

Briais, A., Patriat, P., & Tapponnier, P. (1993). Updated interpretation of magnetic anomalies and seafloor spreading stages in the South China Sea: Implications for the tertiary tectonics of Southeast Asia. *Journal of Geophysical Research*, *98*(B4), 6299–6328. https://doi.org/10.1029/92jb02280

Brun, J. P., & Gutscher, M. A. (1992). Deep crustal structure of the Rhine Graben from DEKORP-ECORS seismic reflection data: A summary. *Tectonophysics*, *208*(1–3), 139–147. https://doi.org/10.1016/b978-0-444-89912-5.50011-9

Brun, J. P., Sokoutis, D., Tirel, C., Gueydan, F., van Den Driessche, J., & Beslier, M. O. (2018). Crustal versus mantle core complexes. *Tectonophysics*, *746*, 22–45. https://doi.org/10.1016/j.tecto.2017.09.017

Buck, W. R. (1988). Flexural rotation of normal faults. *Tectonics*, *7*(5), 959–973. https://doi.org/10.1029/tc007i005p00959

Camanni, G., & Ye, Q. (2022). The significance of fault reactivation on the Wilson cycle undergone by the northern South China Sea area in the last 60 Myr. *Earth-Science Reviews*, *225*, 103893. https://doi.org/10.1016/j.earscirev.2021.103893

Carcione, J. M., & Poletto, F. (2013). Seismic rheological model and reflection coefficients of the brittle–ductile transition. *Pure and Applied Geophysics*, *170*(12), 2021–2035. https://doi.org/10.1007/s00024-013-0643-4

Choi, E., & Buck, W. R. (2012). Constraints on the strength of faults from the geometry of rider blocks in continental and oceanic core complexes. *Journal of Geophysical Research*, *117*(B4), B04410. https://doi.org/10.1029/2011jb008741

Coney, P. J. (1980). Cordilleran metamorphic core complexes: An overview. In *Cordilleran metamorphic core complexes*. (Vol. 153, pp. 7–31). Geological Society of America Memoir. https://doi.org/10.1130/mem153-p7

Deng, H., Ren, J., Pang, X., Rey, P. F., McClay, K. R., Watkinson, I. M., et al. (2020). South China Sea documents the transition from wide continental rift to continental break up. *Nature Communications*, *11*(1), 1–9. https://doi.org/10.1038/s41467-020-18448-y

Edwards, J. H., Kluesner, J. W., Silver, E. A., Brodsky, E. E., Brothers, D. S., Bangs, N. L., et al. (2018). Corrugated megathrust revealed offshore from Costa Rica. *Nature Geoscience*, *11*(3), 197–202. https://doi.org/10.1038/s41561-018-0061-4

Escartín, J., Mevel, C., Petersen, S., Bonnemains, D., Cannat, M., Andreani, M., et al. (2017). Tectonic structure, evolution, and the nature of oceanic core complexes and their detachment fault zones (13 20′ N and 13 30′ N, Mid Atlantic Ridge). *Geochemistry, Geophysics, Geosystems*, *18*(4), 1451–1482.

Gans, P. B., & Gentry, B. J. (2016). Dike emplacement, footwall rotation, and the transition from magmatic to tectonic extension in the Whipple Mountains metamorphic core complex, southeastern California. *Tectonics*, *35*(11), 2564–2608. https://doi.org/10.1002/2016tc004215

Ge, J., Zhu, X., Zhao, X., Liao, J., Ma, B., & Jones, B. G. (2020). Tectono-sedimentary signature of the second rift phase in multiphase rifts: A case study in the Lufeng depression (38–33.9 Ma), Pearl River Mouth Basin, South China Sea. *Marine and Petroleum Geology*, *114*, 104218. https://doi.org/10.1016/j.marpetgeo.2020.104218

Gianelli, G., Manzella, A., & Puxeddu, M. (1997). Crustal models of the geothermal areas of southern Tuscany (Italy). *Tectonophysics*, *281*(3–4), 221–239. https://doi.org/10.1016/s0040-1951(97)00101-7

Hayman, N. W., Grindlay, N. R., Perfit, M. R., Mann, P., Leroy, S., & de Lépinay, B. M. (2011). Oceanic core complex development at the ultraslow spreading Mid-Cayman Spreading Center. *Geochemistry, Geophysics, Geosystems*, *12*(3). https://doi.org/10.1029/2010gc003240

Huang, H., Qiu, X., Zhang, J., & Hao, T. (2019). Low-velocity layers in the northwestern margin of the South China Sea: Evidence from receiver functions of ocean-bottom seismometer data. *Journal of Asian Earth Sciences*, *186*, 104090. https://doi.org/10.1016/j.jseaes.2019.104090

Karson, J. A., Früh-Green, G. L., Kelley, D. S., Williams, E. A., Yoerger, D. R., & Jakuba, M. (2006). Detachment shear zone of the Atlantis massif core complex, mid-Atlantic ridge, 30 N. *Geochemistry, Geophysics, Geosystems*, *7*(6), Q06016. https://doi.org/10.1029/2005gc001109

Klemperer, S.L. (1987). A relation between continental heat flow and the seismic reflectivity of the lower crust. *Journal of Geophysics*, *61*(1), 1–11.

Lecomte, E., Jolivet, L., Lacombe, O., Denèle, Y., Labrousse, L., & Le Pourhiet, L. (2010). Geometry and kinematics of Mykonos detachment, Cyclades, Greece: Evidence for slip at shallow dip. *Tectonics*, *29*(5), TC5012. https://doi.org/10.1029/2009tc002564

Li, C. F., Xu, X., Lin, J., Sun, Z., Zhu, J., Yao, Y., et al. (2014). Ages and magnetic structures of the South China Sea constrained by deep tow magnetic surveys and IODP Expedition 349. *Geochemistry, Geophysics, Geosystems*, *15*(12), 4958–4983. https://doi.org/10.1002/2014gc005567

Liotta, D., & Ranalli, G. (1999). Correlation between seismic reflectivity and rheology in extended lithosphere: Southern tuscany, inner northern Apennines, Italy. *Tectonophysics*, *315*(1–4), 109–122. https://doi.org/10.1016/s0040-1951(99)00292-9

Little, T. A., Webber, S. M., Mizera, M., Boulton, C., Oesterle, J., Ellis, S., et al. (2019). Evolution of a rapidly slipping, active low-angle normal fault, Suckling-Dayman metamorphic core complex, SE Papua New Guinea. *GSA Bulletin*, *131*(7–8), 1333–1363. https://doi.org/10.1130/b35051.1

Lymer, G., Cresswell, D. J., Reston, T. J., Bull, J. M., Sawyer, D. S., Morgan, J. K., et al. (2019). 3D development of detachment faulting during continental breakup. *Earth and Planetary Science Letters*, *515*, 90–99. https://doi.org/10.1016/j.epsl.2019.03.018

Meissner, R., & Strehlau, J. (1982). Limits of stresses in continental crusts and their relation to the depth-frequency distribution of shallow earthquakes. *Tectonics*, *1*(1), 73–89. https://doi.org/10.1029/tc001i001p00073

Mizera, M., Little, T. A., Biemiller, J., Ellis, S., Webber, S., & Norton, K. P. (2019). Structural and geomorphic evidence for rolling-hinge style deformation of an active continental low-angle normal fault, SE Papua New Guinea. *Tectonics*, *38*(5), 1556–1583. https://doi.org/10.1029/2018tc005167

Morley, C. K. (2016). Major unconformities/termination of extension events and associated surfaces in the South China Seas: Review and implications for tectonic development. *Journal of Asian Earth Sciences*, *120*, 62–86. https://doi.org/10.1016/j.jseaes.2016.01.013

Parnell-Turner, R., Escartin, J., Olive, J. A., Smith, D. K., & Petersen, S. (2018). Genesis of corrugated fault surfaces by strain localization recorded at oceanic detachments. *Earth and Planetary Science Letters*, *498*, 116–128. https://doi.org/10.1016/j.epsl.2018.06.034

Platt, J. P., Behr, W. M., & Cooper, F. J. (2015). Metamorphic core complexes: Windows into the mechanics and rheology of the crust. *Journal of the Geological Society*, *172*(1), 9–27. https://doi.org/10.1144/jgs2014-036

Resor, P. G., & Meer, V. E. (2009). Slip heterogeneity on a corrugated fault. *Earth and Planetary Science Letters*, *288*(3–4), 483–491. https://doi.org/10.1016/j.epsl.2009.10.010

Ring, U. (2014). Metamorphic core complexes. *Encyclopedia of marine geosciences*. https://doi.org/10.1007/978-94-007-6644-0_104-4

Sandwell, D. T., Müller, R. D., Smith, W. H., Garcia, E., & Francis, R. (2014). New global marine gravity model from CryoSat-2 and Jason-1 reveals buried tectonic structure. *Science*, *346*(6205), 65–67. https://doi.org/10.1126/science.1258213

Savva, D., Pubellier, M., Franke, D., Chamot-Rooke, N., Meresse, F., Steuer, S., & Auxietre, J. L. (2014). Different expressions of rifting on the South China Sea margins. *Marine and Petroleum Geology*, *58*, 579–598. https://doi.org/10.1016/j.marpetgeo.2014.05.023

Singleton, J. S. (2013). Development of extension-parallel corrugations in the Buckskin-Rawhide metamorphic core complex, west-central Arizona. *The Geological Society of America Bulletin*, *125*(3–4), 453–472. https://doi.org/10.1130/b30672.1

Smith, S. A. F., Holdsworth, R. E., Collettini, C., & Imber, J. (2007). Using footwall structures to constrain the evolution of low-angle normal faults. *Journal of the Geological Society*, *164*(6), 1187–1191. https://doi.org/10.1144/0016-76492007-009

Spencer, J. E. (2011). Gently dipping normal faults identified with Space Shuttle radar topography data in central Sulawesi, Indonesia, and some implications for fault mechanics. *Earth and Planetary Science Letters*, *308*(3–4), 267–276. https://doi.org/10.1016/j.epsl.2011.06.028

Tirel, C., Brun, J. P., & Burov, E. (2008). Dynamics and structural development of metamorphic core complexes. *Journal of Geophysical Research*, *113*(B4), B04403. https://doi.org/10.1029/2005JB003694

Tucholke, B.E., Behn, M.D., Buck, W.R., & Lin, J., (2008). Role of melt supply in oceanic detachment faulting and formation of megamullions. *Geology*, *36*(6), 455–458. https://doi.org/10.1130/G24639A.1

Tucholke, B. E., Lin, J., & Kleinrock, M. C. (1998). Megamullions and mullion structure defining oceanic metamorphic core complexes on the Mid-Atlantic Ridge. *Journal of Geophysical Research*, *103*(B5), 9857–9866. https://doi.org/10.1029/98jb00167

Webber, S., Little, T. A., Norton, K. P., Österle, J., Mizera, M., Seward, D., & Holden, G. (2020). Progressive back-warping of a rider block atop an actively exhuming, continental low-angle normal fault. *Journal of Structural Geology*, *130*, 103906. https://doi.org/10.1016/j.jsg.2019.103906

Wernicke, B., & Axen, G. J. (1988). On the role of isostasy in the evolution of normal fault systems. *Geology*, *16*(9), 848–851. https://doi.org/10.1130/0091-7613(1988)016<0848:otroii>2.3.co;2

Westaway, R., & Kusznir, N. (1993). Fault and bed 'rotation'during continental extension: Block rotation or vertical shear? *Journal of Structural Geology*, *15*(6), 753–770. https://doi.org/10.1016/0191-8141(93)90060-n

Whitney, D. L., Teyssier, C., Rey, P., & Buck, W. R. (2013). Continental and oceanic core complexes. *Geological Society of America Bulletin*, *125*(3–4), 273–298. https://doi.org/10.1130/b30754.1

Wu, G., & Lavier, L. L. (2016). The effects of lower crustal strength and preexisting midcrustal shear zones on the formation of continental core complexes and low-angle normal faults. *Tectonics*, *35*(9), 2195–2214. https://doi.org/10.1002/2016tc004245

Yang, L., Ren, J., McIntosh, K., Pang, X., Lei, C., & Zhao, Y. (2018). The structure and evolution of deepwater basins in the distal margin of the northern South China Sea and their implications for the formation of the continental margin. *Marine and Petroleum Geology*, *92*, 234–254. https://doi.org/10.1016/j.marpetgeo.2018.02.032

Ye, Q., Mei, L., Shi, H., Camanni, G., Shu, Y., Wu, J., et al. (2018). The Late Cretaceous tectonic evolution of the South China Sea area: An overview, and new perspectives from 3D seismic reflection data. *Earth-Science Reviews*, *187*, 186–204. https://doi.org/10.1016/j.earscirev.2018.09.013

Ye, Q., Mei, L., Shi, H., Du, J., Deng, P., Shu, Y., & Camanni, G. (2020). The influence of pre-existing basement faults on the Cenozoic structure and evolution of the proximal domain, northern South China Sea rifted margin. *Tectonics*, *39*(3). https://doi.org/10.1029/2019tc005845

Ye, Q., Mei, L., Shi, H., Shu, Y., Camanni, G., & Wu, J. (2018). A low-angle normal fault and basement structures within the enping sag, Pearl River Mouth Basin: Insights into late mesozoic to early Cenozoic tectonic evolution of the south China sea area. *Tectonophysics*, *731*, 1–16. https://doi.org/10.1016/j.tecto.2018.03.003

Zhao, M. H., Qiu, X. L., Xu, H. L., Xia, K. Y., Shi, X. B., Ye, C. M., & Xia, S. H. (2006). Crustal structure and its low-velocity layer in transition zone of South China Sea. *Journal of Tropical Oceanography*, *25*(5), 36–42. (In Chinese with English abstract).

Zhou, P., Xia, S., Hetényi, G., Monteiller, V., Chevrot, S., & Sun, J. (2020). Seismic imaging of a mid-crustal low-velocity layer beneath the northern coast of the South China Sea and its tectonic implications. *Physics of the Earth and Planetary Interiors*, *308*, 106573. https://doi.org/10.1016/j.pepi.2020.106573

Zhou, Z. (2018). *The Cenozoic crustal thinning and development of hyper-extended rift system in the northern South China Sea*. Ph.D. thesis. China University of Geosciences. Wuhan in Chinese with English abstract.

Zhou, Z., Mei, L., Liu, J., Zheng, J., Chen, L., & Hao, S. (2018). Continentward-dipping detachment fault system and asymmetric rift structure of the Baiyun Sag, northern South China Sea. *Tectonophysics*, *726*, 121–136. https://doi.org/10.1016/j.tecto.2018.02.002

Zhou, Z., Mei, L., Shi, H., & Shu, Y. (2019). Evolution of low-angle normal faults in the Enping sag, the northern South China sea: Lateral growth and vertical rotation. *Journal of Earth Sciences*, *30*(6), 1326–1340. https://doi.org/10.1007/s12583-019-0899-4

Zhu, H., Li, S., Shu, Y., Yang, X., & Mei, L. (2016). Applying seismic geomorphology to delineate switched sequence stratigraphic architecture in lacustrine rift basins: An example from the Pearl River Mouth Basin, northern South China Sea. *Marine and Petroleum Geology*, *78*, 785–796. https://doi.org/10.1016/j.marpetgeo.2015.12.013